Gold nanoparticles deposited on MnO$_2$ nanorods modified graphene oxide composite: A potential ternary nanocatalyst for efficient synthesis of betti bases and bisamides

Pratap S. Nayak[a], Bapun Barik[a], L. Satish K. Achary[a], Aniket Kumar[b], Priyabrat Dash[a,*]

[a] Department of Chemistry, National Institute of Technology Rourkela, Odisha, 769008, India
[b] School of Material Science and Engineering, Chonnam NationalUniversity, Gwang-Ju, Republic of Korea

ARTICLE INFO

ABSTRACT

The decoration of novel nanostructures such as nano particle and nanorod on the surface of graphene oxide (GO) generate potential heterogeneous nanocatalyst. Highlighting this, in the present work, we have designed a ternary GO-MnO$_2$-Au nanocomposite by decorating MnO$_2$nanorods on the surface of graphene oxide via hydrothermal method, followed by deposition of Au nanoparticles on GO-MnO$_2$ surface. The prepared nanocomposite was thoroughly characterised by different instrumental techniques such as X-Ray diffraction (XRD),Fourier transform infrared spectroscopy (FTIR),Raman spectroscopy, Field emission scanning electron microscopy (FESEM), Transmission electron microscopy (TEM), High resolution Transmission electron microscopy (HRTEM), X-Ray photo electron spectroscopy (XPS), N$_2$ adsorption desorption Brunauer–Emmett–Teller (BET) isotherm and Inductively coupled plasma - optical emission spectrometry (ICP-OES). FESEM and TEM images demonstrated that the MnO$_2$ forms rod like structure having diameter of 60–100 nm and are uniformly distributed over the GO surface. HRTEM image clearly signifies gold (Au) nanoparticles having diameter of 7 ± 1.9 nm homogeneously distributed throughout the GO-MnO$_2$ surface. Elementary state of Au and tetravalent nature of Mn as well as reduction of functional group after the decoration was confirmed from XPS studies. The catalyst GO-MnO$_2$-Au was found to be the superior catalyst for synthesis of biologically active molecules such as Betti bases and Bisamides. The high catalytic activity of the materials can be attributed to the small and homogeneous distribution of gold nanoparticles, high redox potential of rod shaped MnO$_2$ and the synergistic effect between GO, MnO$_2$ and Au. All the reaction conditions were optimised by varying catalyst dosage, effect of solvent and temperature. The GO-MnO$_2$-Au was easily recycled with minimal leaching and the product yield was found to be 85–90% after 4th cycle demonstrating the stability and durability of our nanocomposite.

1. Introduction

Syntheses of organic moieties via multicomponent reactions (MCRs) have drawn significant attention due to the process simplicity and time saving operations [1]. In addition, the general features of MCRs match well with green chemistry criteria such as atom economy, waste prevention, avoidance of hazardous compounds, and energy efficiency [2]. Among various multicomponent reactions, the synthesis of Betti base and Bisamide are found to be much crucial due to its unique and wide applications. These compounds are important because of their essential medicinal properties such as anti-inflammatory [3], anti-fungal [4], anti-microbial [5] and anticancer activity [6]. The potential catalysts developed for the synthesis of these compounds are trifluoromethanesulfonic acid (CF$_3$SO$_3$H), boric acid (H$_3$BO$_3$), phosphotungstic acid (H$_3$PW$_{12}$O$_{40}$) [7,8] zinc sulphide (ZnS), nano ferrouso ferric oxide (Fe$_3$O$_4$), triethylamine sulfonic acid (Et$_3$N-SO$_3$H),

iodine, N-methyl-2-pyrrolidone (C$_5$H$_9$NO), N-methyl-2-pyrrolidone (NMP)-HSO$_4$, ionic liquid (IL), ferric hydrogen sulphate (Fe(HSO$_4$)$_3$), cholineper-oxydisulfatemonohydrate (CHPS), and task specific ionic liquids (TSILs) [9–11]. These catalysts have shown many draw backs like lack of environmental safety, use of toxic solvents, recyclability, stability and cost [12]. In addition, to the best of our information, it is still a challenge to use aromatic primary amines as reaction substrates in water owing to their electron-withdrawing properties and steric hindrance [13]. This is because the activity of amine is strongly facilitated with water due to hydrogen bonding with amine. To overcome these problems, lanthanide triflate [14], acid functionalised silica coated magnetic nanoparticles [15] and surfactant [16] were successfully used under water condition or solvent-free condition to synthesize these compounds with high yield. However, these catalysts are not user friendly or not recoverable.

As a consequence, it is beneficial to develop environmentally benign

catalytic processes for Betti reaction. At the same time, synthesis of Bisamides under solvent-free condition is a noteworthy protocol as solvent–free conditions play a crucial role in green chemistry, since there is no need for solvents which are detrimental to the environment [4,17]. Such demand for an environmentally benign procedure with the use of a stable and reusable catalyst encouraged us to develop a safe alternative method for the synthesis of Betti bases and Bisamides. In catalysis, homogeneous catalysts are more efficient than heterogeneous catalysts. However, they have major drawbacks such as high cost, no recovery, and tedious workup. This has triggered the interest more towards heterogeneous catalysts which are cost effective, easily recoverable, and reusable and involve simple procedure to form the product [18,19]. Besides, heterogeneous catalysis has emerged as a useful methodology to reduce waste production owing to the simplicity of the process, lower contamination of the products with the active catalytic species, and less use of toxic solvents [20–22].Owing to their unique properties like high surface-to-volume ratio, high surface area and facile separation, nanostructures of metals and metal oxides have shown great promise as catalysts in many organic reactions. Towards this direction, nano crystalline metal oxides are found to be suitable catalyst for organic reaction [16]. For example, karmakar et al reported an effective approach for synthesis of Betti bases using nano MgO [7]. In another work, nano ZnO was used to synthesize Betti base. One major problem associated with these metal oxides are agglomeration due to their high surface area dispersed in solution which resulted in lower yield of product [23]. However, recent advancements in the synthesis of uniformly sized nanostructures offer numerous opportunities to improve the catalytic performance of these materials [24–26]. This motivated us to develop novel approaches for preparing nano crystalline metal oxides based highly active, recyclable and stable heterogeneous nanocatalyst for the synthesis of Betti base and Bisamides.

Among other metal oxides, manganese dioxide (MnO_2) has been widely used as catalyst owing to its eco-friendly nature, existence of multiple crystalline phases and oxidation states, low cost, high activity, non-toxicity and high redox ability [27,28]. MnO_2 can exist in many polymorphs such as α, β and γ form via the linking of MnO_6 octahedral units [29]. Out of all, β-form exhibit rod like morphology and found to be the most stable form of MnO_2. The presence of large number of surface Mn^{4+} ions, homogeneous distribution, shape anisotropy, high electronic effects and surface unsaturation in MnO_2 nanorods are some of the important factors responsible for its good catalytic activity [30]. However, the increase in surface energy due to large surface area causes various stability issues such as tendency to aggregate, changes in shape, change in surface states leading to an inevitable loss of their original catalytic activities [31,32]. One novel approach to address these issues is found to be the design of composite nanocomposite with other metal nanoparticles such as Pt, Au, Ag and Pd. This type of integration improves the catalytic activity because of synergistic effect between the two components [33–35]. However, it has been shown that such nanocatalyst generally do not retain high catalytic reactivity without a solid support. Generally, they become unstable and structural deformation can occur during the reaction [36]. To address these problems, design of a ternary composite would be an ideal methodology in which the binary composite can be anchored onto a solid support, particularly carbon support. The carbon support will provide permeable pores, chemical inertness, and good mechanical stability where as metal nanoparticle will provide more catalytic centres and further enhance the composite's stability [37–39]. Surprisingly, such ternary heterogeneous composite has drawn little attention in the synthesis of biologically active molecules via MCRs.

Among various carbon materials, graphene oxide has shown great promise as a suitable catalytic support material [40–42].The presence of various oxygen containing functional groups such as hydroxyl, epoxy and carboxyl with large surface area makes GO as a possible support for decoration of catalytically active nanorod and nanoparticle onto it [25,43,44]. At the same time, its high surface area, ultrahigh electrical conductivity, excellent mechanical properties, high thermal conductivity and the lattice defects play an important role in catalysis. The surface defects and oxygen containing functional groups in graphene oxide support can act as strong binding traps for metal nanocatalyst which leads to long term stability of the

material [45,46]. The electronic interaction arising due to the transfer of charge from metal to GO substrate in the composite materials results in the enhancement of its catalytic activity [47,48]. These unique properties of GO fulfil the basic requirements of an ideal catalyst support material. Similarly, among various metal nanoparticles, incorporation of Au nanoparticles can simultaneously enhance charge transfer ability due to local field enhancement and also enhance the stability of the composite due to its chemical stability [49]. Keeping all these factors into mind, it was envisaged that the design of $GO-MnO_2-Au$ will provide a low-cost, stable and efficient heterogeneous nanocatalyst for MCRs. Good electronic interaction between the three components, increased redox potential and possible synergistic effects between them will help to enhance the catalytic activity. Moreover, this methodology will minimize the possibility of nanocatalyst aggregation during recovery and improves the durability of the nanocatalyst [50–52].

Herein, we report the successful demonstration of a nanorod decorated graphene oxide-based $GO-MnO_2-Au$ ternary nanocomposite as a promising heterogeneous catalyst for synthesis of Betti bases and Bisamides. The reaction involves synthesis of amino alkyl napthol and Bisamides by two separate routes from one substrate (aldehydes). The addition of napthol aromatic amines with aromatic aldehydes followed by elimination of water molecules led to the synthesis of amino alkyl napthol (Betti base) whereas condensation of aromatic aldehydes with two molecules of amide led to Bisamides synthesis. All the reactions proceeded with high yields in shorter period of time as compared to other reported catalysts. During the synthesis of Betti bases, higher yield of product was obtained in water solvent using primary aromatic amine as substrate. Similarly, the reaction went well under solvent-free condition during the synthesis of Bisamides. The catalyst can be reused with minimal loss in activity. Our current methodology demonstrates a novel heterogeneous catalyst along with a versatile, stable, green and convenient synthetic protocol that easily afforded the synthesis of Betti bases and Bisamide. Several noticeable benefits are: (1) green reaction condition reaction like water solvent or solvent-free condition; (2) shorter reaction time with high yield, (3) easy catalyst recovery; and (4) easy to handle, safe and stable catalyst with little leaching problem [53,54]. These types of advantages were not obtained in some of the reported literatures. Moreover, our current study can be successfully extended to the synthesis of other important multicomponent reactions.

2. Experimental Section

2.1. Materials

$HAuCl_4$, $MnSO_4$ and $KMnO_4$, were purchased from Hi-Media. Graphite powder, H_3PO_4 and H_2O_2were purchased from Sigma-Aldrich. $NaBH_4$, ethanol, $NaNO_3$, H_2SO_4 (98%), HCl and silica gel were purchased from Avra Chemicals. All chemicals were used as received without further purification.

2.2. Preparation of GO

Graphene oxide was prepared from the graphite flakes by modified Hummer's method. Firstly 1.4 g graphite flakes was taken in a 1000 ml round bottom flask followed by addition of 2 g $NaNO_3$ and 40 ml sulphuric acid. After adding all, the mixture was continuously stirred in ice-cold (0–5 °C) bath. The solution was stirred for 2 h followed by adding $KMnO_4$ carefully and maintaining the temperature below 14 °C. Then, the solution was brought to room temperature. After some time, the solution became pasty brownish and then again stirred for 2 h. During constant stirring, temperature increased in each half an hour and then 100 ml water was added resulting in the change of colour to brown. Later on, 200 ml water was added and then stirred continuously. The solution was finally treated with 20 ml H_2O_2 to terminate the reaction with formation of yellow colour. The solution was purified by centrifugation and rinsed with HCl and with DI water for various times. After filtration it was dried overnight in oven to get the synthesized GO.
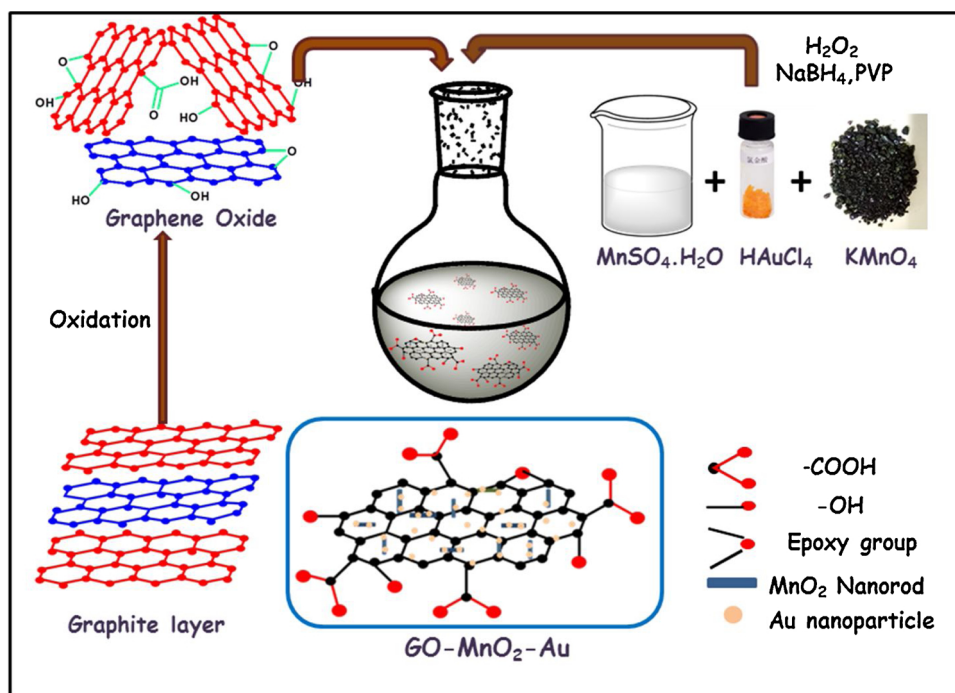
Scheme 1. Synthesis scheme of catalyst GO-MnO$_2$-Au.
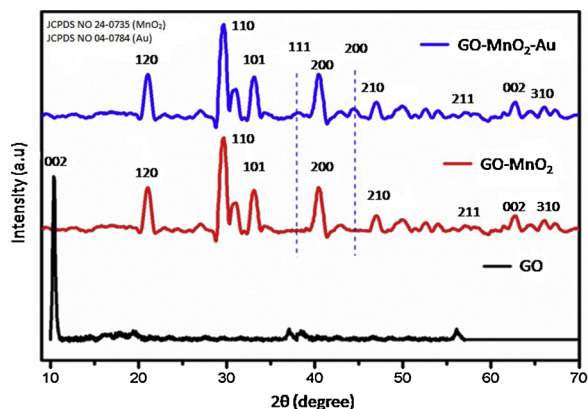
Fig. 1. XRD spectra of GO, GO-MnO$_2$ and GO-MnO$_2$-Au.
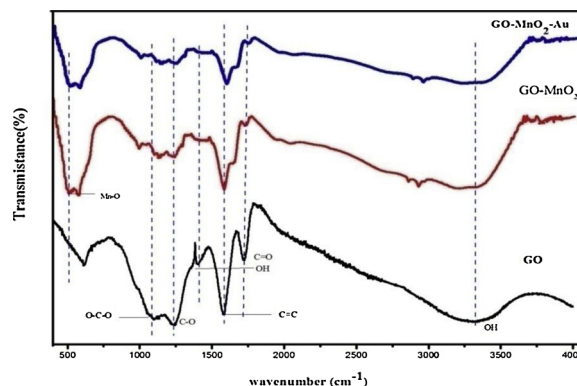
Fig. 2. FTIR spectra of GO, GO-MnO$_2$ and GO-MnO$_2$-Au.

2.3. Preparation of GO-MnO$_2$ nanorod composite

In a typical system, 0.016 g of MnSO$_4$·H$_2$O were mixed with 0.23 g of GO in distilled water (50 ml) and then ultra-sonicated for 2 h forming a brown homogeneous solution. In this procedure, Mn^{2+} of MnSO$_4$.H$_2$O bond to the negative O atom present in functional groups of GO through electrostatic interaction. Then, KMnO$_4$ solution was prepared by dissolving 0.32 g of KMnO$_4$ in 50 ml distilled water. The obtained KMnO$_4$ solution was added to the MnSO$_4$.H$_2$O solution under constant vigorous stirring. After that whole solution was transferred to the autoclave, sealed and heated at 120 °C for 12 h. After completion of reaction, the solution was brought to room temperature. The formed brown-black precipitates were collected and washed several times with ethanol to remove the excess of impurities.

2.4. Preparation of GO-MnO$_2$-Au composite

In brief, 96 mg of GO-MnO$_2$ was taken in 50 ml of distilled water followed by addition of 0.1 ml of 0.01 M prepared poly vinyl pyrrolidone (PVP) solution. The solution was stirred and heated to boiling. Then, 12 ml of 1 wt% HAuCl$_4$ solution was added quickly under nitrogen atmosphere

and stirred for 30 min. After that 20 ml sodium borohydride (NaBH$_4$) solution (0.01 M) was added slowly under constant stirring for 20 min for reduction of gold salt. The resulting solution was stirred for 6 h under nitrogen atmosphere at 80 °C and then cooled to room temperature. After that it was centrifuged and washed several times with water to remove impurities. Then the resulting material was dried in the oven to get desired GO-MnO$_2$-Au nanocomposite (Scheme 1).

2.4.1. General procedure for synthesis of Betti base

In a typical procedure, benzaldehyde, 2-napthol and aniline having same ratio (1 mmol) were taken in a round bottom flask and mixed and stirred at room temperature, followed by the addition of GO-MnO$_2$-Au (15 mg) catalyst in water. The progress of the reaction was monitored by thin layer chromatography (TLC). After completion of reaction, the catalyst was separated by centrifugation and then washed and dried for further use. The unreacted materials present in the product were removed by washing with water and dissolved in ethyl acetate. The final pure product was separated by column chromatography.

2.4.2. General procedure for synthesis of Bisamides

Briefly, 1 milimole of benzaldehyde and 2 milimole of acetamide were taken in a round bottom flask followed by addition of a catalytic
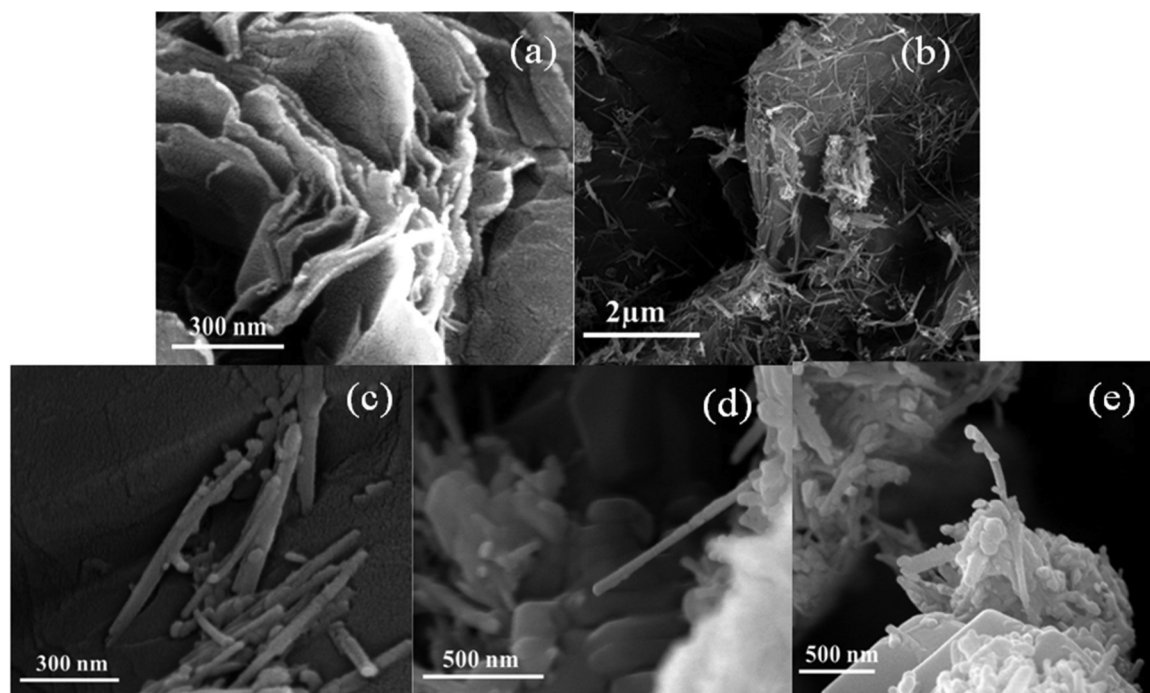
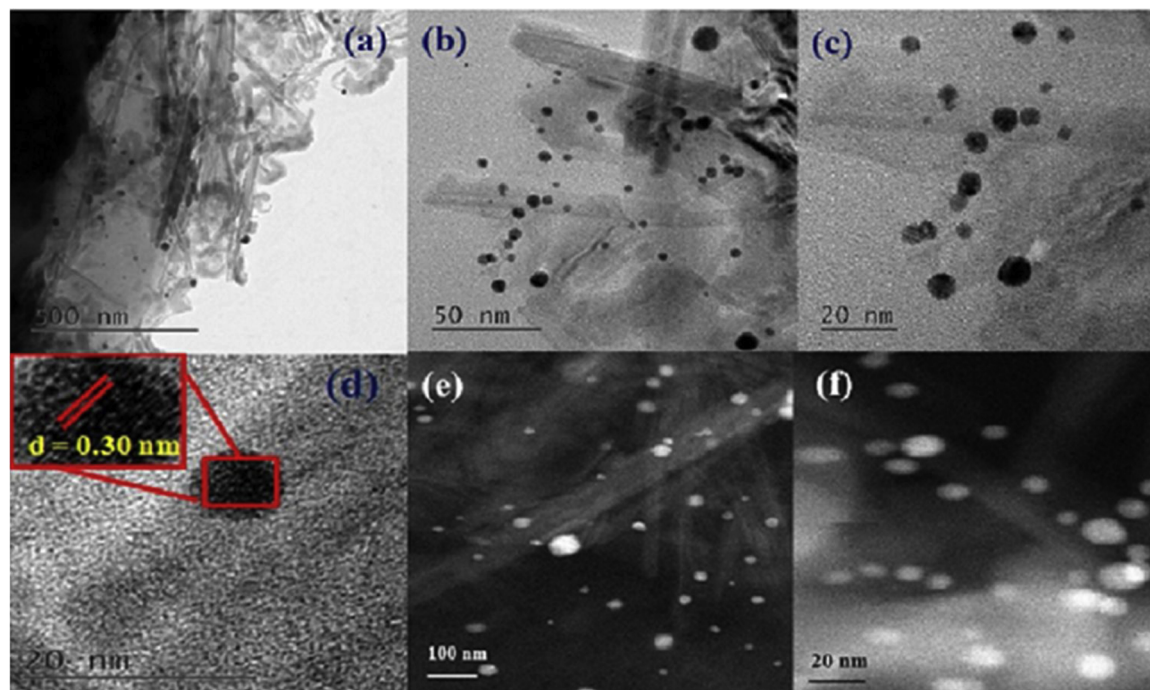**Fig. 3.** FESEM images of (a) GO (b) GO-MnO$_2$ and (c–f) GO-MnO$_2$-Au.

Fig. 4. (a–d) TEM images of GO-MnO$_2$-Au and (e, f) HRTEM images of GO-MnO$_2$-Au.

amount of GO-MnO$_2$-Au (15 mg) in solvent-free condition at 80°C. The progress of the reaction was checked by TLC. After the reaction was completed, product was separated out and washed and then dissolved in ethyl acetate. The final product was separated by column chromatography.

3. Characterisations

FTIR spectra of the product were recorded using a Perkin-Elmer-1000 FTIR spectrophotometer using NaCl support. XRD patterns were analysed by using Rigaku, ultimate-iv, japan multipurpose X-ray diffraction system with Ni filtered Cu-Kα source. The composition information was measured using EDX (JEOL JSM-6480LV). Raman spectra were recorded using a BRUKER RFS 27 spectrometer. Transmission electron micrographs (TEM) of the sample were recorded using PHILIPS CM 200 equipment using carbon coated copper grids. Field emission scanning electron microscopy (FESEM) of the sample was recorded by Nova Nano SEM/FEI-450. Nitrogen adsorption/desorption isotherm was obtained at 77 K on a Quantachrome Autosorb-IQ 3-B apparatus. The specific surface area and pore size distribution were acquired by emulating BET equation and BJH method, respectively. ^{1}H NMR and ^{13}C NMR spectra were recorded on a Bruker spectrometer at
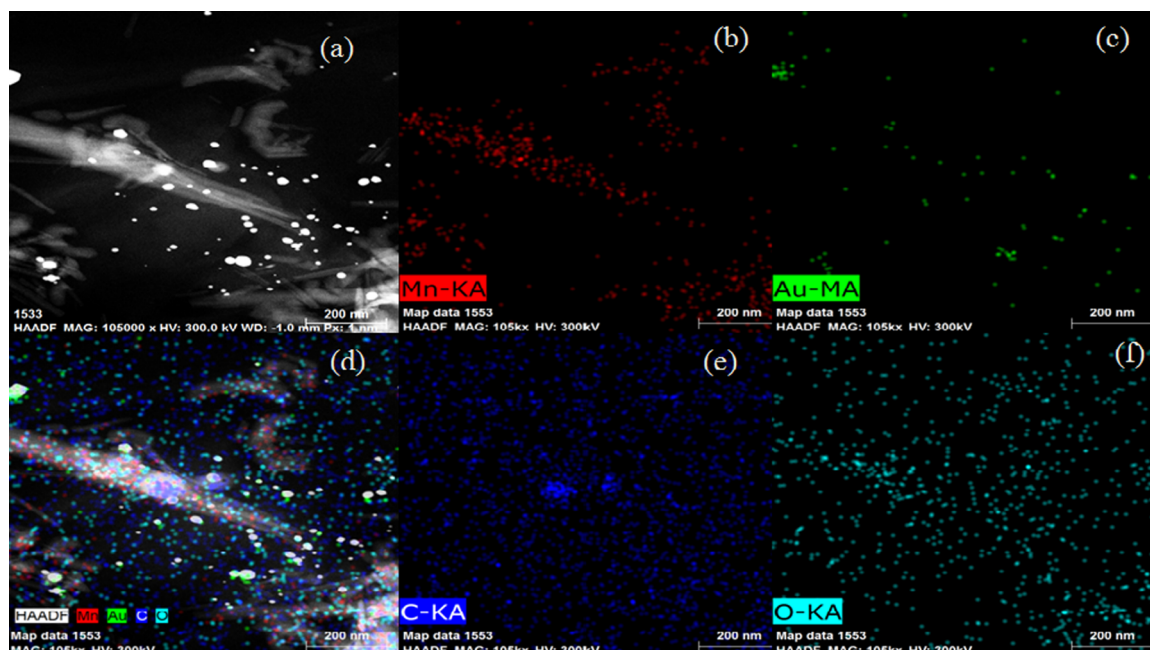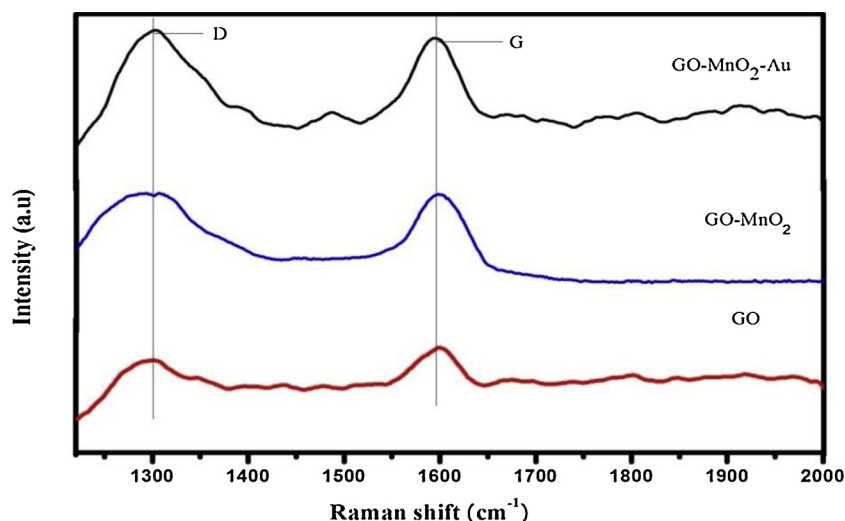
Fig. 5. (a-f) Elemental mapping of GO-MnO$_2$-Au.

Fig. 6. Raman spectra of GO, GO-MnO$_2$ and GO-MnO$_2$-Au.

Table 1
Surface area and pore volume of GO,GO-MnO$_2$ and for GO-MnO$_2$-Au.

Catalyst	Surface area (g^2. m^{-1})	Pore volume (nm)
MnO$_2$	58	3.2
GO-MnO$_2$	132	5.8
GO-MnO$_2$-Au	118	5.3

400 MHz using TMS as an internal standard. A commercial electron energy analyzer(PHOIBOS 150 from Specs GmbH, Germany) and a non-monochromatic Mg Kα X-ray source have been used to perform XPS measurements with the base pressure of 10 mbar supplied by Thermo-scientific, UK, equipped with an Al Ka (1486.6 eV). Catalytic reactions were monitored by thin layer chromatography on 0.2 mm silica gel F-254 plates. ICP-OES were performed using Perkin Elmer (Optima2100 DV) in the range of 0.005–100.0 mg/L. All the reaction products are known compounds and were identified by comparing their physical and spectral characteristics with the literature reported values.

4. Results and discussion

The MnO$_2$ nanorod was decorated on GO surface via hydrothermal method. During the synthesis of GO-MnO$_2$ composite, initially, large number of nuclei aggregated into a mixture of α and γ form of MnO$_2$ having dendrites structure. With time this structure broke down into micro rods and phase transformation occur leading to the formation of β-form of MnO$_2$ [55].The suggests that β-MnO$_2$ is the most thermo-dynamically stable form of MnO$_2$. During the formation, following reaction takes place:

$$3Mn^{2+} + 2MnO_4^- + 2H_2O \rightarrow MnO_2 + 4H^+$$
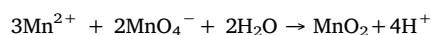
The ternary nanocomposite (GO-MnO$_2$-Au) was then synthesized by simple reduction of gold salt onto the GO-MnO$_2$ composite. As the morphology of nanoparticles and their distribution on the surfaces of nanorods are critical to the catalytic properties, care was taken to uniformly modify the surfaces of nanorods with monodispersed nano-particles. In the ternary composite, GO provides the stability to MnO$_2$
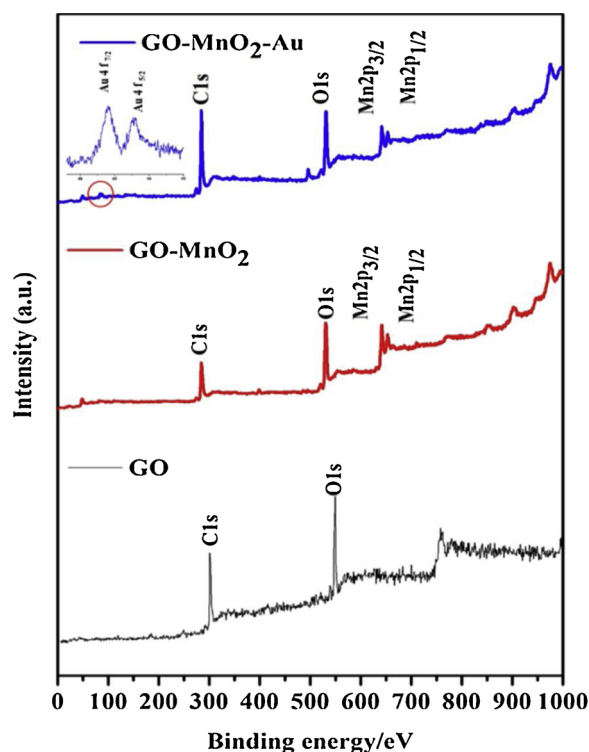
Fig. 7. XPS Survey scan study of GO, GO-MnO$_2$ and GO-MnO$_2$-Au.

and Au by making different types of electrostatic interaction with oxygen containing functional groups. Because of such interaction, the catalytic properties of the ternary composite could substantially improved as discussed in the catalytic studies section. Later on, to check the successful synthesis of MnO$_2$ nanorod, decoration of these rods on GO structure, the presence of functional groups on GO and the successful synthesis of the desired ternary nanocatalyst, various characterization techniques were utilized and the results are outlined below.

Initially, the phase purity and presence of functional groups on the nanocomposite were investigated by XRD and FTIR techniques. Fig. 1 shows the XRD patterns of individual GO, GO-MnO$_2$ and GO-MnO$_2$-Au composite. The diffraction peaks at 110,110, 101, 200, 210, 211, 002 and 310 matches with the β-form of MnO$_2$ (JCPDS 24-0735). However, the relative intensities of peaks were found to be higher than other reported MnO$_2$ particle, which reveals the formation of rod like morphology. XRD peaks of GO shows a broad diffraction peak at 2θ = 10.89° corresponding to (002) plane which is very large compared to the graphite. No distinct peaks of GO was observed in both GO-MnO$_2$ and GO-MnO$_2$-Au which may be due to incorporation of MnO$_2$ and Au nanoparticles in between GO layers. After the deposition of gold nanoparticles on GO-MnO$_2$, the obtained XRD patterns remains almost unchanged with weak metallic gold diffraction lines at 38.33° and 44.56° which are assigned to face-cantered cubic (fcc) bulk gold (111) and (200) planes, respectively.

FTIR spectra were carried out to study the presence of various functional groups in the GO-MnO$_2$-Au nanocomposite. Fig. 2 shows the FTIR spectra of GO, GO-MnO$_2$ and GO-MnO$_2$-Au. The broad absorption peak at 3419 cm^{-1} in the spectra of GO can be attributed to the stretching vibration of −OH group. The peaks corresponding to

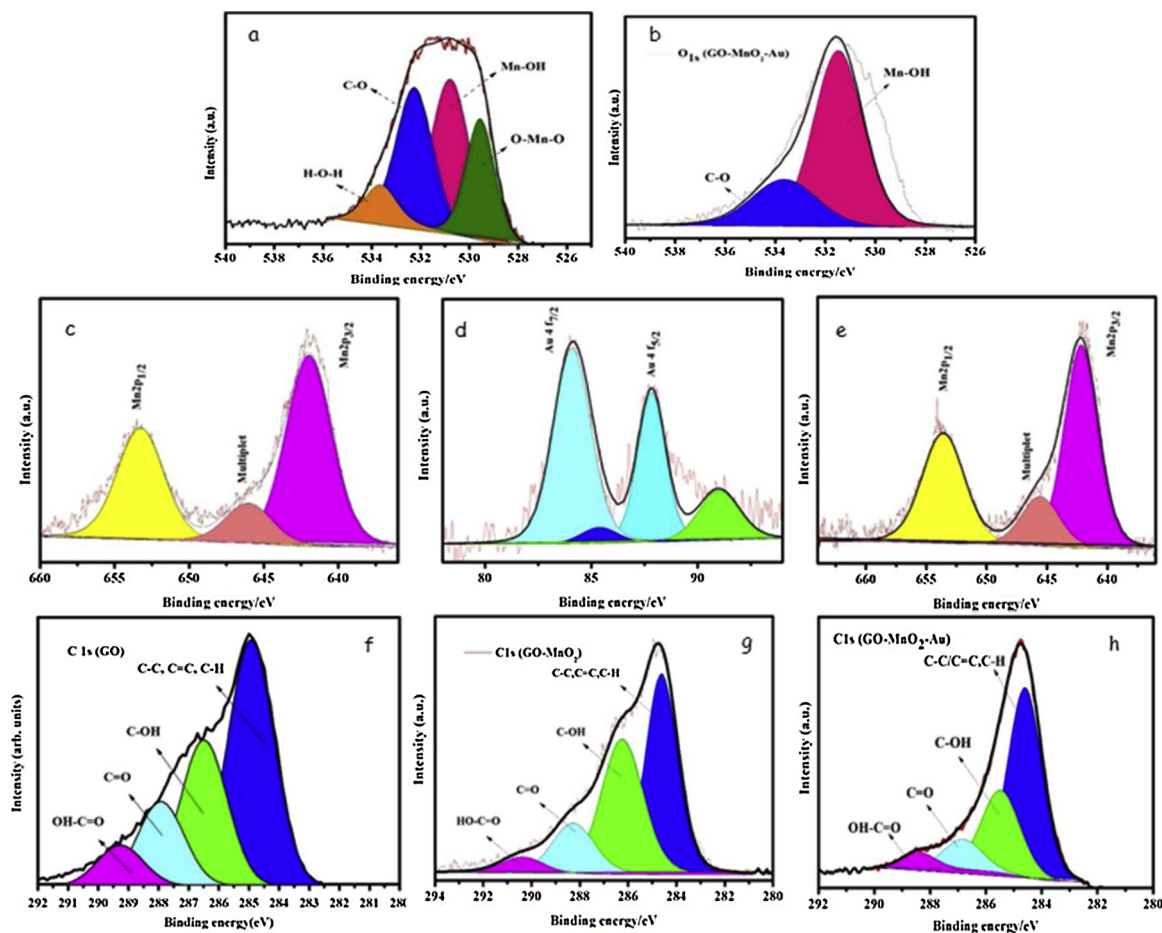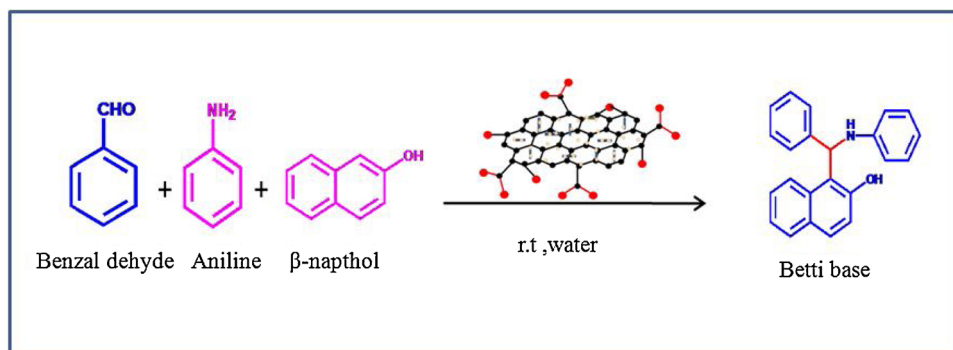**Fig. 8.** XPS spectra (a,b) O 1s XPS spectra of GO-MnO$_2$ and GO-MnO$_2$-Au, (c and e) Mn 2p spectra of GO-MnO$_2$ and GO-MnO$_2$-Au, (d) 4f spectra of Au, (f, g, h) C 1s XPS spectra of GO,GO-MnO$_2$ and GO-MnO$_2$-Au.

Scheme 2. Reaction scheme for synthesis of Betti base.

Table 2
Effect of catalyst for synthesis of Betti base synthesis.

Entry	Solvent	Catalyst	Catalyst loading	Time(min.)	Temp.($^{\circ}$C)	Yield (%)
1	Water	–	–	180	rt	Trace
2	Water	GO	2O wt(%)	50	rt	50
3	Water	GO-MnO$_2$	2O wt(%)	25	rt	80
4	Water	GO-MnO$_2$-Au	2O wt(%)	10	rt	96
5	Water	MnO$_2$	2O wt(%)	39	rt	66

Reaction condition :- Benzaldehyde (1 mmol),2-napthol (1 mmol), and aniline (1 mmol), catalyst (15 mg),water solvent, rt.

Table 4
Effect of metal oxide loading (MnO$_2$ with respect to GO) for Betti base synthesis.

Entry	Solvent	Catalyst	Catalyst loading	Time (min.)	Temp.($^{\circ}$C)	Yield (%)
1	Water	GO-MnO$_2$	5 wt(%)	48	rt	41
2	Water	GO-MnO$_2$	10 wt(%)	40	rt	52
3	Water	GO-MnO$_2$	15 wt(%)	31	rt	71
4	Water	GO-MnO$_2$	20 wt(%)	25	rt	80
5	Water	GO-MnO$_2$	25 wt(%)	25	rt	79
6	Water	GO-MnO$_2$	30 wt(%)	27	rt	77

Reaction condition :- Benzaldehyde (1 mmol),2-napthol (1 mmol), and aniline (1 mmol), GO-MnO$_2$-Au (15 mg),water solvent, rt.

over both rods and also on GO sheet. After deposition of MnO$_2$ nanorods and gold nanoparticles, the layer structure of GO was still maintained. The rod shape and structure of gold nanoparticles in the nanocomposite were further confirmed from the TEM images.

TEM analysis is one of the most important techniques to understand the structural morphology of a nanomaterial. TEM images shown in Fig. 4a further reveal that the MnO$_2$ have well-defined rod like morphology. The lattice fringes of the β-MnO$_2$ nanorods shown in the high-resolution TEM (HRTEM, Fig. 4d) image indicate the high crystalline nature of these nanorods, and the measured lattice spacing is confirmed to be 0.30 nm, which is consistent with the d-spacing of the (200) plane of the tetragonal β-MnO$_2$ crystal [57]. Gold nanoparticles are found to be spherical in shape and are highly dispersed on the GO-MnO$_2$ surface which prevent the restacking of GO layer, leading to the enahanced stability of GO. Gold particle sizes are estimated to be 7 ± 1.9 nm. To find out the distribution of MnO$_2$ on GO and Au on GO-MnO$_2$ nanocomposite, elemental mapping of the nanocomposite were carried out. Fig. 5b and c depicts the elemental mapping of gold, manganese, carbon and oxygen. From the elemental mapping of manganese it is clearly seen that it forms a rod like structure. From the elemental mapping of gold it is clear seen that gold particles are homogeneously distributed over GO and MnO$_2$ in the ternary composite.

To understand the formation any surface defects, degree of

1732 cm^{-1} attributed to carbonyl group of carboxyl (C=O), 1372 cm^{-1} associated to phenol and alcohol groups, 1263 cm^{-1} attributed to epoxy and ether groups, 1595 cm^{-1} to C=C and 1065 cm^{-1} to C–O–C groups. In the IR spectrum of GO-MnO$_2$, stretching vibrations of C–O–C and O–H peaks reduced due to reduction of some oxygen containing functional groups during deposition of MnO$_2$. Further, one additional peak was observed at 597 cm^{-1} that is assigned to Mn-O stretching vibration [56] confirming the successful decoration of MnO$_2$ nanorods on GO. After deposition of gold nanoparticles the intensities of the peaks remains almost same and the external and internal structure of GO-MnO$_2$-Au was further studied by FESEM and TEM.

FESEM is a powerful technique to investigate the surface morphology of a sample. Fig. 3 shows the FESEM images of GO, GO-MnO$_2$ and GO-MnO$_2$-Au. It is clear from FESEM image that the layer structure with sub micrometre pore is visible in the case of pure GO (Fig. 3a). From Fig. 3, it can be seen that MnO$_2$ forms rods like morphology and are homogeneously distributed throughout GO surface. The diameter of the rods is found to be in the range of 60–100 nm and length around 400–600 nm. In Fig. 3c, gold nanoparticles are found to be dispersed

Table 3
Effect of solvent for synthesis of Betti base synthesis.

Entry	Solvent	Catalyst	Catalyst loading	Time(min.)	Temp.($^{\circ}$C)	Yield (%)
1	Hexane	GO-MnO$_2$-Au	20wt(%)	15	rt	56
2	THF	GO-MnO$_2$-Au	20wt(%)	21	rt	72
3	Acetonitrile	GO-MnO$_2$-Au	20wt(%)	19	rt	75
4	DCM	GO-MnO$_2$-Au	20wt(%)	18	rt	63
5	Toluene	GO-MnO$_2$-Au	20wt(%)	15	rt	43
6	Methanol	GO-MnO$_2$-Au	20wt(%)	15	rt	81
7	Water	GO-MnO$_2$-Au	20wt(%)	10	rt	96

Reaction condition :- Benzaldehyde (1 mmol),2-napthol (1 mmol), and aniline (1 mmol), GO-MnO$_2$-Au (15 mg), rt.

Table 5

Effect of metal nanoparticle loading (Auwith respect to GO-MnO$_2$) for Betti base synthesis.

Entry	Solvent	Catalyst	Catalyst loading	Time(min.)	Temp.(°C)	Yield (%)
1	Water	GO-MnO$_2$-Au	0.5 wt(%)	18	rt	88
2	Water	GO-MnO$_2$-Au	1.0 wt(%)	10	rt	96
3	Water	GO-MnO$_2$-Au	1.5 wt(%)	11	rt	96
4	Water	GO-MnO$_2$-Au	2.0 wt(%)	13	rt	95

Reaction condition :- Benzaldehyde (1 mmol),2-napthol (1 mmol), and aniline (1 mmol), GO-MnO$_2$-Au (15 mg),water solvent, rt.

Table 6

Effect of catalytic loading of GO-MnO$_2$-Au for Betti base synthesis.

Entry	Solvent	Catalyst	Catalyst amount (mg)	Time(min.)	Temp.(°C)	Yield (%)
1	Water	GO-MnO$_2$-Au	5	16	rt	85
2	Water	GO-MnO$_2$-Au	10	13	rt	89
3	Water	GO-MnO$_2$-Au	15	10	rt	96
4	Water	GO-MnO$_2$-Au	20	11	rt	95
5	Water	GO-MnO$_2$-Au	25	12	rt	95

Reaction condition :- Benzaldehyde (1 mmol), 2-napthol (1 mmol), and aniline (1 mmol), GO-MnO$_2$-Au (15 mg),water solvent, rt.

hybridisation, crystal order and extent of chemical modification in the nanocomposite, Raman measurements were then carried out. Raman spectroscopy could possibly give useful information in the GO-MnO$_2$-Au nanocomposite in comparison to GO and GO-MnO$_2$ due to the enhanced disorder created in it. In Raman spectra of graphene oxide (Fig. 6), two major peaks were observed near 1340 cm^{-1} and 1592 cm^{-1}, corresponding to the well-documented D and G bands, respectively. The D band at 1340 cm^{-1} arises due to the defect induced in the sp^2 ring of graphitic materials due to oxidation and G band is due to first order scattering of E$_{2g}$ phonons of sp^2 carbon [58]. The larger intensity and line width of D band than G band signifies more disorder in the structures due to defects. When MnO$_2$ was decorated on GO sheet its I$_D$/I$_G$ value increased (0.98) with respect to GO (0.96) indicating the formation of slight disorderness in the structure. This suggests that electronic interaction occurred on deposition of MnO$_2$ nanorod on GO sheet. Further, while decorating gold nanoparticles on composites the intensity ratio of D and G band remains almost same while little broadening of peak happened. This possibly represents the damage in the structure due to the electron-phonon coupling by Au ions [59].

Surface area of nanocomposite plays an important role in catalysis by providing more surface active sites on which more number of reactants can be adsorbed. In order to find out the surface area, the N$_2$ adsorption- desorption studies were carried out for GO, GO-MnO$_2$ and GO-MnO$_2$-Au and the results are shown in Fig. S1. It was found that all the samples show type-IV isotherm. The average pore diameters in MnO$_2$, GO–MnO$_2$ and GO-MnO$_2$-Au composite were found to be 3.2 nm, 5.8 nm and 5.3 nm, respectively whereas BET surface areas were 58 m^2 g^{-1}, 132 m^2 g^{-1}, and 118 m^2 g^{-1}, respectively (Table 1). The increase in surface area after decorating MnO$_2$ on GO can be attributed to the reduction of oxygen functional groups during the synthesis while further deposition of gold nanoparticles blocked the pore size resulting in the decrease of the surface area [60].

Later on, the chemical composition and oxidation state of metals in GO-MnO$_2$-Au were analysed by X-ray photo electronic spectroscopy (XPS).The presence of all the elements C, O, Mn and Au in GO-MnO$_2$-Au were confirmed from the survey scan XPS spectra (Fig. 7). The C1 s core level XPS spectrum of GO (Fig. 8e) consist of four main peaks out of which two peaks at284.5 and 286.7 eV, corresponds to C=C/C-C (sp^2) of aromatic rings and C−OH of hydroxyl groups. Other two peaks at 287.8 and 289.1 eV corresponds to keto group (C=O) of carbonyl and carboxyl groups. After the decoration of MnO$_2$ on GO (Fig. 8f) and Au on GO-MnO$_2$ (Fig. 8g) surface, decrease in intensities of oxygen containing functional groups were found due to the binding of metal (Mn and Au) with oxygen containing functional groups [61,62] and due to reduction of oxygen functional groups during the synthesis. Mn 2p

spectrum of GO-MnO$_2$ and GO-MnO$_2$-Au shown in Fig. 8 (c, e) depicts two peaks at 641.6 and 654.4 eV assigned to Mn 2p$_{3/2}$ and Mn 2p$_{1/2}$, respectively. The two peaks observed for Mn is due to spin orbit coupling with an energy separation of 12.8 eV which confirmed that the Mn in GO-MnO$_2$ and GO-MnO$_2$-Au remained tetravalent (Mn^{4+}) [63,64]. It can also be seen that the 2p peaks of Mn in GO-MnO$_2$-Au decreased to small extent possibly due to deposition of Au nanoparticles on MnO$_2$ surface. Two peaks observed for O1 s at 529.7 eV and 532.6 eV is due to Mn-O and oxygen containing functional groups associated with GO. All the above data clearly reveals that successful decoration of MnO$_2$ nanorod on GO surface. The decrease in peaks of oxygen containing functional groups suggests the presence of a strong chemical interaction between Mn with GO surface which was previously confirmed from FTIR analysis. Fig. 8d shows the high resolution XPS spectra of Au 4f in which two distinct peaks separated by 3.6 eV can be seen which suggests the spin orbit coupling of 4f orbital. The two peaks at 87.81 eV and 84.24 eV corresponds to Au 4f$_{7/2}$ and 4f$_{5/2}$ in GO-MnO$_2$-Au samples which indicates that gold is found to be in metallic form (Au^0) [63].The peaks of 4f$_{7/2}$ was shifted to 0.2 eV from the metallic gold reported in literature which further suggest the possible electron interaction between the species in the nanocomposite. After successful characterization, the potential and efficiency of the designed nanocatalyst (GO-MnO$_2$-Au) as active and stable catalyst was investigated in the synthesis of Betti bases and Bisamides.

5. Catalytic study

5.1. Synthesis of Amino alkylnapthol (Betti base)

The catalytic efficiency of GO-MnO$_2$-Au was then investigated in the multicomponent reactions of aldehydes, aniline and β-naphol to synthesize amino alkylnapthol (Scheme 2). To get the optimisation condition, the reaction of benzaldehyde, aniline and β-napthol was taken as the model reaction. Initially, different catalysts were investigated in water media in order to find out the suitable catalyst for synthesis of amino alkyl napthol. When no catalyst was used trace amount of product was obtained (entry 1, Table 2). Then, we investigated the reaction under homogeneous catalytic conditions using MnSO$_4$.H$_2$O, KMnO$_4$, and HAuCl$_4$.3H$_2$O. However, they did not show any good activity under these conditions. To study the heterogeneous systems, we examined the catalytic reactivity of unsupported MnO$_2$ catalyst (Table 2 and 8 (entry 5). The reaction took longer time in both the cases. When we tested the catalytic performance of GO supported GO-MnO$_2$ and GO-MnO$_2$-Au under identical reaction conditions, better yield of the product was obtained. From this experiment it can be inferred that the nanorods
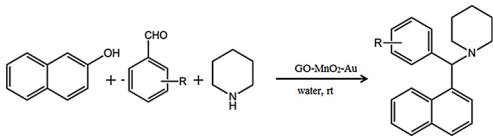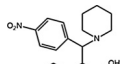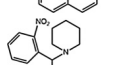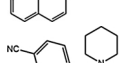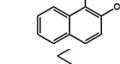
Table 7
Effect of different substrate for synthesis of Betti base synthesis.

Entry	Aldehyde	Product	Time	Yield
1	P-NO$_2$		7	95
2	P-Br		9	95
3	P-OMe		13	88
4	P-C$_2$H$_5$		13	88

Entry	Aldehyde	Product	Time	Yield
5	P-OMe		11	93
6	M,P-OMe		12	93
7	O.M,P-OMe		13	95
8	P-C$_2$H$_5$		9	93
9	P-Cl		8	94
10	P-Br		9	13
11	H		7	96

Table 7 (*continued*)

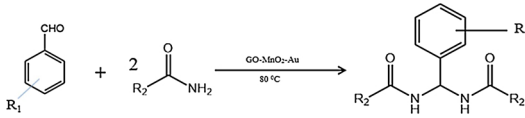| Entry	Aldehyde		Product	Time	Yield
12	P-NO$_2$			7	95
13	O-NO$_2$			8	95
14	P-CN			9	94
15	H	C$_4$H$_9$NH$_2$		14	89

Reaction condition: Benzaldehyde (1 mmol),2-napthol (1 mmol), and aniline (1 mmol), GO-MnO$_2$-Au (15 mg),water solvent, rt.
Reaction condition: Benzaldehyde (1 mmol),2-napthol (1 mmol), and pyrrolidine (1 mmol), GO-MnO$_2$-Au (15 mg),water solvent, rt.
Reaction condition: Benzaldehyde (1 mmol),2-napthol (1 mmol), and piperidine (1 mmol), GO-MnO$_2$-Au (15 mg),water solvent, rt.

Table 8
Effect of catalyst for synthesis of Bisamide synthesis.

Entry	Catalyst	Catalyst loading	Solvent	Temp.(^{o}C)	Time (min.)	Yield (%)
1	–	–	Solvent less	80	90	Trace
2	GO	15 wt(%)	Solvent less	80	44	23
3	GO-MnO$_2$	15 wt(%)	Solvent less	80	21	75
4	GO-MnO$_2$-Au	15 wt(%)	Solvent less	80	4	97
5	MnO$_2$	15 wt(%)	Solvent less	80	32	58

Reaction condition: - Benzaldehyde (1 mmol), and acetamide (2 mmol), catalyst (15 mg), solventless, 80 $^{\circ}$C.
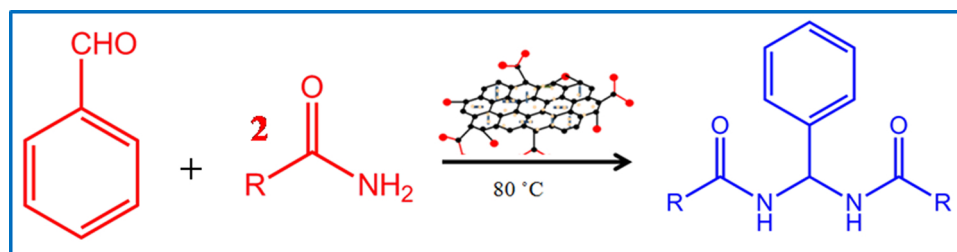

Scheme 3. Reaction scheme for synthesis of Bisamide.

Table 9
Effect of solvent for synthesis of Bisamide synthesis.

Entry	Solvent	Catalyst	Catalyst loading	Time(min.)	Temp.(^{o}C)	Yield (%)
1	Hexane	GO-MnO$_2$-Au	15 wt(%)	15	80	48
2	THF	GO-MnO$_2$-Au	15 wt(%)	21	80	61
3	Acetonitrile	GO-MnO$_2$-Au	15 wt(%)	19	80	69
4	DCM	GO-MnO$_2$-Au	15 wt(%)	18	80	53
5	Water	GO-MnO$_2$-Au	15 wt(%)	15	80	82
6	Methanol	GO-MnO$_2$-Au	15 wt(%)	15	80	75
7	Solvent less	GO-MnO$_2$-Au	15 wt(%)	4	80	97

Reaction condition: - Benzaldehyde (1 mmol), and acetamide (2 mmol), GO-MnO$_2$-Au (15 mg), 80 $^{\circ}$C.
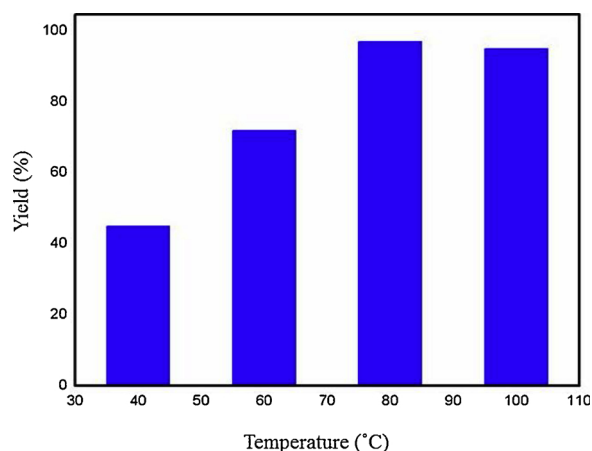
Fig. 9. Effect of temperature with yield for synthesis of bisamides. Reaction condition : Benzaldehyde (1 mmol), and acetamide (2 mmol), GO-MnO$_2$-Au (15 mg), solventless, 80 °C.

Table 10
Effect of metal oxide loading (MnO$_2$ with respect to GO) for Bisamide synthesis.

Entry	Catalyst	Catalyst loading	Solvent	Temp.(°C)	Time (min.)	Yield (%)
1	GO-MnO$_2$	5 wt (%)	Solvent less	80	35	51
2	GO-MnO$_2$	10 wt (%)	Solvent less	80	29	69
3	GO-MnO$_2$	15 wt (%)	Solvent less	80	21	75
4	GO-MnO$_2$	20 wt (%)	Solvent less	80	22	74
5	GO-MnO$_2$	25 wt (%)	Solvent less	80	25	74

Reaction condition: - Benzaldehyde (1 mmol), and acetamide (2 mmol), GO-MnO$_2$-Au (15 mg), solventless, 80 °C.

supported on stable support provide a higher product yield in less time. However, highest yield (96%) of the desired product was obtained in presence of GO-MnO$_2$-Au as catalyst (entry 4, Table 2) which tells that ternary composite is superior to that of a binary compound. Catalysts are strongly influenced by solvents because of polarity, protictity (hydrogen bond forming ability) and basicity. On account of this, we had investigated the role of solvent by varying the solvent media for the model reaction and the result is summarised in Table 3. Both polar and non-polar solvents are used for optimisation. It was found that less product yield (56%) obtained in nonpolar solvent (Table 3 entry1) whereas the yield of the product increased moderately in solvents like tetra hydro furan (THF), dichloro methane (DCM), toluene and acetonitrile (Table 3 entry 2–6). The yield of Betti reaction increased with increase in polarity of the solvent and water shows high affinity towards this reaction because it can form hydrogen bonding, charge stabilisation and dipolar effects [65–67]. Additionally, solubility of substrate in water is high and formation of transition state would be sooner.

After optimising the solvent media, all other optimisations were done by taking water as media. The effect of MnO$_2$ on product yield was investigated by changing the loading of MnO$_2$ from 5 to 30 % (Table 4, entries 1–5). It was observed that the yield of the product increased

from 41 to 80% and then remained almost constant with further increase in loading. The constant or slight decrease in catalytic properties is due to the agglomeration of nanorods which cover the active site in the ternary composite [68]. This result motivated us to modify the Au loading to improve the reaction rate as well as product yield. To get high yield of product in a fixed amount we varied the weight percentage (wt %) of Au from 0.5 to 2.0 with respect to GO-MnO$_2$and found that at 1 wt% catalyst show high yield of 96% (Table 5, entries 2).Further, to check the effect of amount of GO-MnO$_2$-Au catalyst, the amount was varied and found that 15 mg (Table 6, entry 3) as the optimised catalyst for synthesis of amino alkyl napthol. The reaction was also carried out in solvent-free condition at room temperature but the yield of the product was not satisfactory at room temperature. Thus, the optimised catalyst for the synthesis of Betti base was; 15 mg of 20 wt % of MnO$_2$ with respect to GO and 1 wt% of gold with respect to GO-MnO$_2$ in water medium at room temperature. The Mn and Au loading on the above optimised nanocatalyst, measured by ICP-OES, was found to be ˜12.73 wt % and ˜ 0.96 wt%, respectively. The mol% of the metal catalyst was found to be 3.48 mol % Mn and 0.08 mol% Au from ICP-OES analysis in the ternary composite [69–71]. After the optimisation of catalyst, a series of products were then synthesized by taking aldehyde as a substrate. Encouraged by this success, to further evaluate the scope of this reaction, different aromatic aldehydes, amines, 2-napthol and amides were used under similar conditions (Tables 7 and 13).Aldehydes with functionality gave much satisfactory results, however groups like NO$_2$, Br and Cl were found to be more reactive and completed the reaction in shorter period of time (Table 7, entry 1,2 and 9). Benzamides were found to be highly reactive than acetamide that might be due to more basicity of Benzamides. It was observed that the substituent at para position ((Table 13, entry 3) showed better yields as compared to that at ortho positions (Table 13,entry 7).

5.2. Synthesis of Bisamides

Similarly, the reaction between benzaldehyde and acetamide was taken as a model reaction to get the optimisation conditions for the synthesis of Bisamide (Scheme 3). Here, at first the effect of different type of catalysts was investigated. The reaction was allowed to proceed both in absence and presence of catalyst in solvent-free conditions at 80 °C and it was found that the presence of catalysts is essential for the reaction. The yield was found to be less in presence of GO (23%) as compared to GO-MnO$_2$ (74%) and GO-MnO$_2$-Au (97%) (Table 8 entries 1–4).

Later on, the reaction in different polar, non-polar and also in solvent-free condition was carried out. The highest product yield was found in case of reaction occurring in solvent-free condition as compared to solvent media (Table9, entry7). Temperature is an essential parameter which has a greater impact on reaction progress. To investigate the effect of temperature on catalytic activity of GO-MnO$_2$-Au, the temperature was varied. It was found that with rise in temperature the product yield was increased up to 80 °C and then for further increase in temperature yield remained almost same (Fig. 9).

To get the optimised condition for the amount of active centres like MnO$_2$ and Au on GO surface, the wt% of both the elements were then varied. The yield of product was found to increase from 51% to 75%

Table 11
Effect of metal nanoparticle loading (Au with respect to GOMnO$_2$)) for Bisamide synthesis.

Entry	Catalyst	Catalyst loading	Solvent	Temp.(°C)	Time (min.)	Yield (%)
1	GO-MnO$_2$-Au	0.5 wt (%)	Solvent less	80	8	70
2	GO-MnO$_2$-Au	1.0 wt (%)	Solvent less	80	4	97
3	GO-MnO$_2$-Au	1.5 wt (%)	Solvent less	80	6	95
4	GO-MnO$_2$-Au	1.5 wt (%)	Solvent less	80	9	94

Reaction condition: - Benzaldehyde (1 mmol), and acetamide (2 mmol), GO-MnO$_2$-Au (15 mg), solventless, 80 °C.

Table 12
Effect of catalytic loading of GO-MnO$_2$-Au for Bisamide synthesis.

Entry	Catalyst	Catalyst loading(mg)	Solvent	Temp.(°C)	Time (min.)	Yield (%)
1	GO-MnO$_2$-Au	5	Solvent less	80	11	80
2	GO-MnO$_2$-Au	10	Solvent less	80	6	87
3	GO-MnO$_2$-Au	15	Solvent less	80	4	97
4	GO-MnO$_2$-Au	20	Solvent less	80	5	95

Reaction condition: - Benzaldehyde (1 mmol), and acetamide (2 mmol), GO-MnO$_2$-Au (15 mg), solventless, 80 °C.

with the increase in MnO$_2$ loading on GO from 5% to 15% (Table10, entries 1–3) and almost remained same on further increase in wt% of MnO$_2$ with respect to GO. With increasing gold loading the yield of the reaction was increased linearly up to 1 wt% after which the yield increased slightly. The increased activity was due to the presence of active sites of gold nanoparticles [72] whereas decreased activity was due to covering of Au nanoparticles on the active site of MnO$_2$ nanorods and also agglomeration of Au nanoparticles [73,74]. From the investigation it was found that 1 wt% of gold with respect to GO-MnO$_2$ shows high activity (97% yield) towards the synthesis of Bisamides under solvent-free condition at 80 °C(Table 11,entries1–4). Later on, to optimise the amount of catalyst we had varied the amount from 5 to 20 mg (Table 12 entry 3) and found that 15 mg shows better yields with less time. Therefore, the optimised conditions for the synthesis of Bisamides were: 15 mg of 15 wt (%) of MnO$_2$ with respect to GO and 1 wt% of gold with respect to GO-MnO$_2$in solvent-free condition at 80 °C. The Mn and Au loading on the above optimised nanocatalyst, measured by ICP-OES, was found to be ˜9.49 wt% and ˜ 0.95 wt%, respectively. From same ICP-OES study, the mol% of the metal catalyst was found to be 2.60 mol % Mn and 0.079 mol% Au in the ternary composite [69–71,75]. After optimisation of the catalyst, the scope and limitations of this procedure were studied by carrying out a series of reactions by taking aldehydes as variable substrates (Table 13).The reactions went well with a good product yield with almost all the aldehydes. However, it was seen from the investigation that electron withdrawing group at para position of benzaldehyde accelerate the rate of reaction for Bisamide synthesis.

To demonstrate the advantages of our catalyst for the synthesis of biologically important molecules such as Betti bases and Bisamides, we compared the activity of our catalyst with other reported catalyst and the data is summarised in table (Table14 and 15). Our catalyst shows better results than other reported catalyst like high yield in less reaction time, environmental friendly and green conditions. For example, when we compare the activity, stability and reactivity with other reported catalyst like TiO$_2$, ZnS and CTAB (Table 14, entry 3–5) for Betti base synthesis we found high yield (96%) of products in shorter period of time. Moreover, stability and recyclability is an issue in thee reported systems. Similarly, for the synthesis of Bisamides, some of the previously used catalysts involve acid catalysts or ionic liquid based catalysts like SiO$_2$-IL and CHPS-TSIL (Table 15, entry 7, 8). However, acid catalysts are not environmental friendly while ionic liquids are quite expensive. Thus it can be confirmed that our catalyst (GO-MnO$_2$-Au) is more superior for synthesis of both Betti bases and Bisamides with superior properties.

From all the above data it can be concluded that GO-MnO$_2$-Au catalyst showed higher activity in comparison to other systems. The tetravalent nature of Mn in MnO$_2$ and high redox ability (due to reduction of Mn^{7+} and oxidation of Mn^{2+} to Mn^{4+}) play an important role for such increased catalytic activity [76]. Significant enhancement of catalytic property after deposition of gold nanoparticles is due to highly dispersion and small size of gold nanoparticles on surface of GO-MnO$_2$ [77]. Electric dipole is the driving force in case of O = Mn = O for homogeneous distribution of Au nanoparticles. When gold nanoparticles are decorated on MnO$_2$ surface its redox potential values increases drastically leading to increase in catalytic property [78]. Besides, due to the high surface area of our nanocomposite as observed
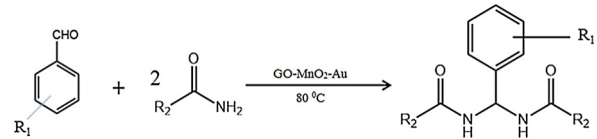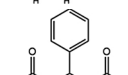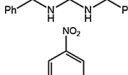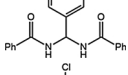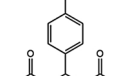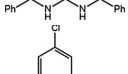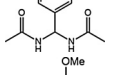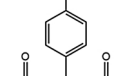
from BET measurements, it adsorbs more reactant molecules on to it through π-π stacking and electro static interaction leading to enhancement in catalytic property [79]. In the end, when MnO$_2$ and Au nanoparticles are decorated over graphene oxide sheet it shows high activity possibly due to synergistic effects between GO,MnO$_2$ and Au. To study such synergi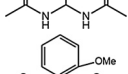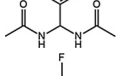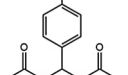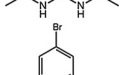stic effect, the catalytic activity of both prepared nanocomposite and the physical mixture of its individual components were tested. It was found that the reaction containing GO-MnO$_2$-Au nanocomposite shows highest yield in both the synthesis of Betti base (96% yield) and Bisamides (97% yield) whereas the product yield was found to be less in case of physical mixture of all the three components such as GO, MnO$_2$ nanorod and Au for the synthesis of both Betti bases (73% yield) and Bisamides (78% yield). Therefore, all in all, the higher catalytic activity of GO-MnO$_2$-Au can be attributed to high redox potential of MnO$_2$, small and homogeneous distribution of Au nanoparticles, high surface area and possible synergistic effect between GO and MnO$_2$ nanorod as well as Au nanoparticles [80–84].

Heterogeneous nature of catalyst is the most important point of research in catalysis. These heterogeneous catalysts are generally composed of one or more catalytically active components and a functional support, in which the interaction between the catalytic components and the support materials endow composite catalysts with much improved catalytic properties, such as significantly enhanced catalytic activity, selectivity for target products, chemical stability and prolonged lifetime [18,85–89]. Such enhancement was seen in our cases where GO supported binary and tertiary composite showed higher activity than that of unsupported systems (Table 2 and 8, entry. 7). To further confirm the heterogeneity of our catalyst, a leachibility study of was done. For this a hot filtration test was carried out by taking benzaldehyde (1 mmol), β-napthol (1 mmol) and aniline (1 mmol) for amino alkyl napthol and benzaldehyde (1 mmol) and acetamide (2 mmol) for Bisamides synthesis. The synthesis of amino alkyl napthol reaction was performed at room temperature for 5 min in water solvent. After that catalyst was filtered in hot condition and the yield of product was found to be 52%. No further yield beyond 55% is observed after 10 min of the reaction. For synthesis of Bisamides, the reaction was performed for 2 min and yield was found to be 57%. Similar to above, the catalyst was then filtered in hot condition and reaction was continued with the filtrate. Small increase in yield upto 60% was found after 10 min. No further increase in yield after filtration suggests the heterogeneous nature of our catalyst.

5.3. Reproducibility

Reusability and durability of the catalysts are important factors for practical applications [90]. To verify these issues, we investigated separation, leaching and recycling of the GO-MnO$_2$-Au catalyst (Table 16). The catalyst after one reaction were recovered by centrifugation and washed with water and ethanol, then dried and reused for another reaction under the same conditions. The catalyst was successfully recycled and reused for four consecutive cycles with small decrease in activity. The product yield was found to be 86% and 88% for Bisamides and Betti bases from 96% and 97% respectively. The ICP-OES analysis indicated very small amount of metal i.e. 0.08% Mn and 0.186 wt% Au during Betti base reaction while 0.06 wt% Mn and

Table 13
Effect of substrate variation for Bisamide synthesis.

Entry	Aldehydes (R$_1$)	Amides (R$_2$)	Product	Time	Yield
1	H	CH$_3$		7	96
2	H	Ph		5	97
3	P-NO$_2$	Ph		4	97
4	P-Cl	Ph		6	95
5	P-Cl	CH$_3$		10	93
6	P-OMe	CH$_3$		12	91
7	O-OMe	CH$_3$		14	90
8	P-F	CH$_3$		9	94
9	P-Br	CH$_3$		11	93
10	P-C$_2$H$_5$	CH$_3$		16	88
11	P-OEt	CH$_3$		13	86
12	P-OMe	Ph		10	92

Reaction condition :-Benzaldehyde (1 mmol), and acetamide (2 mmol), GO-MnO$_2$-Au (15 mg), solventless, 80 °C.

0.162 wt% Au during Bisamides were leached. These results indicate the remarkable stability of catalyst. FESEM and TEM image of the re-cycled catalyst showed that the catalyst was stable after the recycling (Fig. S2). Therefore, the small decrease of catalytic activity seems to result from either incomplete separation of the GO-MnO$_2$-Au catalyst or leaching of Mn and Au species during the successive recycling.

5.4. Probable reaction mechanism

The mechanism of these multicomponent reactions generally pro-ceeds through addition as well condensation route (Scheme 4 and 5). The Lewis acidic property of our catalyst GO-MnO$_2$-Au catalyst acti-vates the carbonyl oxygen of aldehydes and form an intermediate which then reacts with aniline (in Betti reaction) and acetamide (in Bisamides)

Table 14
Comparisation with other catalyst for Betti base synthesis.

Entry	Catalyst	Solvent	Temp.(°C)	Time	Yield (%)
1	TsOH	Solventless	rt	4.0 (hrs.)	35
2	Boric acid	Solventless	rt	4.5 (hrs.)	15
3	TiO$_2$	Solventless	rt	4.0 (hrs.)	25
4	ZnS	Solventless	rt	4.5 (hrs.)	13
5	CTAB	Solventless	rt	5.2(hrs.)	59
6	Nano Fe$_3$O$_4$	Solventless	rt	4.0 (hrs.)	74
7	Nano MgO	Water	rt	1.5(hrs.)	62
8	ZnO NPs	Water	rt	4.0 (hrs.)	12
9	ZnO reverse micelle (100 nm)	Water	rt	1 (hrs.)	98
10	ZnO reverse micelle (200 nm)	Water	rt	30 (min)	96
11	Cerium(iv) nitrate	Methanol	rt	30 (min)	96
12	GO-MnO$_2$-Au	Water	rt	10(min)	96

Table 15
Comparisation with other catalyst for Bisamide synthesis.

| Entry	Catalyst	Solvent	Temp (°C)	Time	Yield (%)
1	CF$_3$SO$_3$H	MDC	Reflux	0.2-48h	67-98
2	H$_3$BO$_3$	Tolune	Reflux	16-80h	38-92
3	TEA sulfonic acid	Neat	110	15-50min	86-96
4	Iodine	Tolune	125	30min	93
5	NMP HSO$_4$	Neat	100	3min	90
6	SiO$_2$-IL	Neat	85	5min	92
7	CHPS-TSIL	Neat	70	5-20min	88-97
8	GO-MnO$_2$-Au	Solvent less	80	4min	97

Table 16
Recyclibility of catalyst GO-MnO$_2$-Au for sour successive runs.

(a)Recyclibity Test for synthesis of Betti bases.
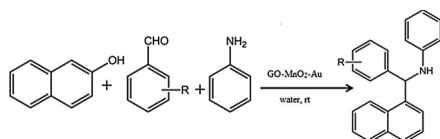
cycle	1	2	3	4
Yield of product (%) for Betti base[a]	97	95	91	88

(b) Recyclibity test foe synthesis of Bisamide
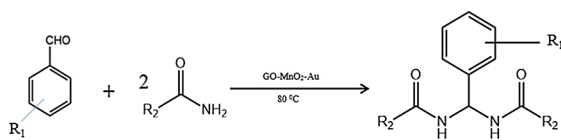

| cycle	1	2	3	4
Yield of the product (%) For Bisamide[b]	96	93	89	86

Reaction condition : (a) Benzaldehyde (1 mmol),2-napthol (1 mmol), and aniline (1 mmol), GO-MnO$_2$-Au (15 mg),water solvent, rt.
Reaction condition : (b) Benzaldehyde (1 mmol), and acetamide (2 mmol), GO-MnO$_2$-Au (15 mg), solventless, 80 °C.

to generate imine and acyl imminium intermediates respectively after dehydration [13,91].The intermediate imine further adsorbed on surface of catalyst and activated by metals (Mn and Au). More electrophilic nature of intermediate fascinate the nucleophilic addition of 2-napthol to give desired product and regenerates the catalyst. The product Bisamide obtained after the removal of catalyst from acyliminium intermediate followed by addition of one more molecule of amide. Formation of intermediate in both cases is the rate determine step. The syengergstic effects between GO, MnO$_2$ and Au in GO-MnO$_2$-Au helps to enhance the catalytic property. Lewis acidic nature of catalyst accepts
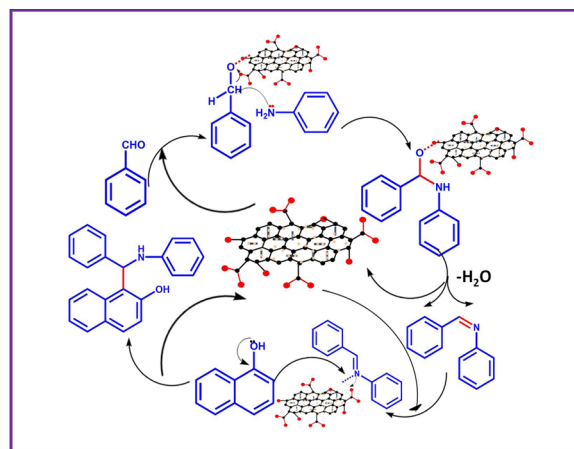
Scheme 4. Mechanistically synthesis of Betti base.
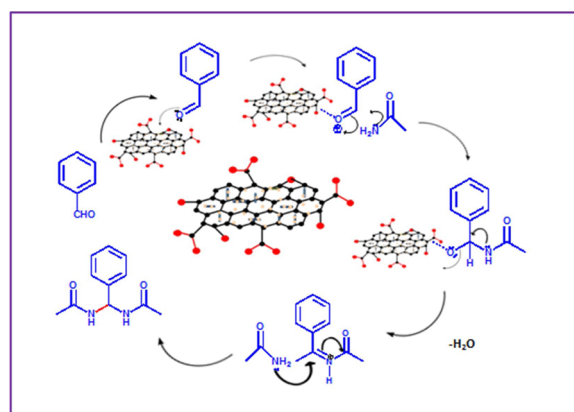
Scheme 5. Mechanistically synthesis of Bisamide.

the electron from oxygen atom of substrate (aldehyde) and form coordinate bond which activates the reaction. After that the metal gold and metal oxide nanorod of MnO$_2$ plays crucial role to accelerate the catalytic activity by electronic effect. In addition, solvent water helps to stabilise the reactants by forming hydrogen bond that play a role in enhancement of the catalytic activity.

6. Conclusions

In summary, ternary GO-MnO$_2$-Au nanocomposite was successfully synthesized by hydrothermal route and used as a catalyst for the one pot multicomponent synthesis of Betti bases and Bisamides using aldehydes as a substrate. Synthesis of Betti bases showed better results at room temperature in water as a solvent while synthesis of Bisamides showed at 80 °C in solvent free condition. The formation of nanorods and β form of MnO$_2$ were confirmed by FESEM, TEM and XRD. The diameter of the rods was found to be 60–100 nm and average size of the gold nanoparticles was found to be 7 ± 1.9 nm. The oxidation state of Mn (+ 4) and Au (0) was confirmed from XPS. The linkage between Mn-O and also small reduction of functional group present over GO were confirmed from XPS and FTIR. Both the biological active compounds were synthesized by ternary composite with shorter time in green water solvent and solvent-free conditions. The high activity of the catalyst can be attributed to high redox potential with uniform rod shapes of MnO$_2$, small and uniform dispersion of gold nanoparticles and synergistic effect between GO, MnO$_2$ and gold nanoparticles.

Appendix A. Supplementary data

Supplementary material related to this article can be found, in the online version, at doi:https://doi.org/10.1016/j.mcat.2019.110415.

References

[1] B.L. Gadilohar, H.S. Kumbhar, G.S. Shankarling, New J. Chem. 39 (2015) 4647–4657.
[2] L. Reguera, Y. Méndez, A.R. Humpierre, O. Valdés, D.G. Rivera, Acc.Chem.Res. 51 (2018) 1475–1486.
[3] J.W. Collet, K. Ackermans, J. Lambregts, B.U. Maes, R.V. Orru, E. Ruijter, J. Org. Chem. 83 (2018) 854–861.
[4] K. Gong, H. Wang, X. Ren, Y. Wang, J. Chen, Green Chem. 17 (2015) 3141–3147.
[5] N. Deibl, R. Kempe, Angew. Chem. 56 (2017) 1663–1666.
[6] L.M. Aguirre-Díaz, F. Gándara, M. Iglesias, N. Snejko, E. Gutiérrez-Puebla, M.Á. Monge, J.Am.chem.soc 137 (2015) 6132–6135.
[7] B. Karmakar, J. Banerji, Tetrahedron Lett. 52 (2011) 4957–4960.
[8] J. Legros, J.R. Dehli, C. Bolm, Adv. Synth.Catal. 347 (2005) 19–31.
[9] F. Zhou, Y.L. Liu, J. Zhou, Adv. Synth. Catal. 352 (2010) 1381–1407.
[10] A. Olyaei, E. Sadat Abforushha, R. Khoeiniha, Lett.Org. 14 (2017) 103–108.
[11] S.A. Ramachandran, P.S. Jadhavar, S.K. Miglani, M.P. Singh, D.P. Kalane, A.K. Agarwal, B.D. Sathe, K. Mukherjee, A. Gupta, S. Haldar, Bioorg. Med. Chem. Lett. 27 (2017) 2153–2160.
[12] T.V. Mahrova, G.K. Fukin, A.V. Cherkasov, A.A. Trifonov, N. Ajellal, J.-F. Carpentier, Inorg. Chem. 48 (2009) 4258–4266.
[13] J. Mou, G. Gao, C. Chen, J. Liu, J. Gao, Y. Liu, D. Pei, RSC Adv. 7 (2017) 13868–13875.
[14] S. Kobayashi, H. Ishitani, S. Komiyama, D.C. Oniciu, A.R. Katritzky, Tetrahedron Lett. 37 (1996) 3731–3734.
[15] H. Moghanian, A. Mobinikhaledi, A. Blackman, E. Sarough-Farahani, RSC Adv. 4 (2014) 28176–28185.
[16] A. Kumar, M.K. Gupta, M. Kumar, Tetrahedron Lett. 51 (2010) 1582–1584.
[17] M. Shokouhimehr, K. Hong, T.H. Lee, C.W. Moon, S.P. Hong, K. Zhang, J.M. Suh, K.S. Choi, R.S. Varma, H.W. Jang, Green Chem. 20 (2018) 3809–3817.
[18] M. Shokouhimehr, Catalysts 5 (2015) 534–560.
[19] X.-Z. Shu, S.C. Nguyen, Y. He, F. Oba, Q. Zhang, C. Canlas, G.A. Somorjai, A.P. Alivisatos, F.D. Toste, J. Am. Chem. Soc. 137 (2015) 7083–7086.
[20] D. Rasina, A. Kahler-Quesada, S. Ziarelli, S. Warratz, H. Cao, S. Santoro, L. Ackermann, L. Vaccaro, Green Chem. 18 (2016) 5025–5030.
[21] K.-H. Choi, M. Shokouhimehr, Y.-E. Sung, Bull. Korean Chem. Soc. 34 (2013) 1477–1480.
[22] N. Nitta, F. Wu, J.T. Lee, G. Yushin, Mater. today 18 (2015) 252–264.
[23] A. Punnoose, K. Dodge, J.W. Rasmussen, J. Chess, D. Wingett, C. Anders, ACS susta. chem. eng. 2 (2014) 1666–1673.
[24] A. Kumar, L. Rout, L.S.K. Achary, R.S. Dhaka, P. Dash, Sci. Rep. 7 (2017) 42975–42983.
[25] X. Huang, Z. Zhao, L. Cao, Y. Chen, E. Zhu, Z. Lin, M. Li, A. Yan, A. Zettl, Y.M. Wang, Science 348 (2015) 1230–1234.
[26] M. Shokouhimehr, M.S. Asl, B. Mazinani, Res. Chem. Intermediat. 44 (2018) 1617–1626.
[27] F. Cheng, Y. Su, J. Liang, Z. Tao, J. Chen, Chem.Mater. 22 (2009) 898–905.
[28] Z. Awan, K.S. Nahm, J.S. Xavier, Biosen.Bioelectron. 53 (2014) 528–534.
[29] Q. Yu, J. Xu, C. Wu, J. Zhang, L. Guan, ACS Appl. Mater. Interfaces 8 (2016) 35264–35269.
[30] Y. Pi, Z. Li, D. Xu, J. Liu, Y. Li, F. Zhang, G. Zhang, W. Peng, X. Fan, ACS Sustaina. Chem. Eng. 5 (2017) 5175–5182.
[31] Z. Chen, G. Li, H. Zheng, X. Shu, J. Zou, P. Peng, Appl. Surf. Sci. 420 (2017) 205–213.
[32] X. Cui, Z. Hua, L. Chen, X. Zhang, H. Chen, J. Shi, ChemSusChem 9 (2016) 1010–1019.
[33] M. Kohantorabi, M.R. Gholami, New.J.Chem. 41 (2017) 10948–10958.
[34] M. Shokouhimehr, T. Kim, S.W. Jun, K. Shin, Y. Jang, B.H. Kim, J. Kim, T. Hyeon, Appl.Catal.A 476 (2014) 133–139.
[35] H. Alamgholiloo, S. Zhang, A. Ahadi, S. Rostamnia, R. Banaei, Z. Li, X. Liu, M. Shokouhimehr, Mol Catal. 467 (2019) 30–37.
[36] L. Liu, P. Concepción, A. Corma, J.Catal 340 (2016) 1–9.
[37] J. Asgardi, J.C. Calderón, F. Alcaide, A. Querejeta, L. Calvillo, M.J. Lázaro, G. García, E. Pastor, Appl. Catal.B 168 (2015) 33–41.
[38] S.W. Jun, M. Shokouhimehr, D.J. Lee, Y. Jang, J. Park, T. Hyeon, Chem. Comm. 49 (2013) 7821-782.
[39] M. Shokouhimehr, J.-H. Kim, Y.-S. Lee, Synlett 2006 (2006) 0618–0620.
[40] O.C. Compton, S.T. Nguyen, small 6 (2010) 711–723.
[41] M. Gómez-Martínez, A. Baeza, D.A. Alonso, Catalysts 7 (2017) 94–102.
[42] R.K. Layek, M.E. Uddin, N.H. Kim, A.K.T. Lau, J.H. Lee, Compos B. Eng. 128 (2017) 155–163.
[43] S. Song, X. Wang, H. Zhang, NPG Asia Mater. 7 (2015) 179–188.
[44] M.G. Álvarez, D.G. Crivoi, F. Medina, D. Tichit, Chem.Eng. 3 (2019) 29–37.

[45] H. Ahmad, M. Fan, D. Hui, Compos. B. Eng. 145 (2018) 270–280.
[46] K. Zhang, K. Hong, J.M. Suh, T.H. Lee, O. Kwon, M. Shokouhimehr, H.W. Jang, Res.Chem.Intermediat 45 (2019) 599–611.
[47] B. Şen, E.H. Akdere, A. Şavk, E. Gültekin, Ö. Paralı, H. Göksu, F. Şen, Appl. Catal. B 225 (2018) 148–153.
[48] K. Zhang, K. Hong, J.M. Suh, T.H. Lee, O. Kwon, M. Shokouhimehr, H.W. Jang, Res.Chem. Intermediat. 45 (2019) 599–611.
[49] A. Lolli, R. Amadori, C. Lucarelli, M.G. Cutrufello, E. Rombi, F. Cavani, S. Albonetti, Microporous Mesoporous Mater. 226 (2016) 466–475.
[50] L.H. Lu-Cun Wang, Qian Liu, Yong-Mei Liu, Miao Chen, Yong Cao, He-Yong He, Kang-Nian Fan, Appl. Catal. A Gen. 344 (2008) 150–157.
[51] A. Ying, S. Liu, Z. Li, G. Chen, J. Yang, H. Yan, S. Xu, Adv. Synth. Catal. 358 (2016) 2116–2125.
[52] Q. Yue, Y. Zhang, C. Wang, X. Wang, Z. Sun, X.-F. Hou, D. Zhao, Y. Deng, J. Mater. Chem. 3 (2015) 4586–4594.
[53] Y. Ping, J. Zhang, T. Xing, G. Chen, R. Tao, K.-H. Choo, J.ind.eng. chem 58 (2018) 74–79.
[54] M.T. Islam, R. Saenz-Arana, H. Wang, R. Bernal, J.C. Noveron, New J.Chem. 42 (2018) 6472–6478.
[55] D. Su, H.-J. Ahn, G. Wang, NPG Asia Mater. 5 (2013) 70–78.
[56] A. Grimaud, O. Diaz-Morales, B. Han, W.T. Hong, Y.-L. Lee, L. Giordano, K.A. Stoerzinger, M.T. Koper, Y. Shao-Horn, Nat. Chem. Biol. 9 (2017) 457–465.
[57] N. Tang, X. Tian, C. Yang, Z. Pi, Q. Han, J.Phys. Chem. Solids 71 (2010) 258–262.
[58] N. Tang, X. Tian, C. Yang, Z. Pi, Q. Han, J.Phys.Chem. Solids 71 (2010) 258–262.
[59] J. Mondal, M. Marandi, J. Kozlova, M. Merisalu, A. Niilisk, V. Sammelselg, J. Chem. Eng. 8 (2014) 786–793.
[60] L. Chen, J. Hu, R. Richards, J. Am. Chem. Soc. 131 (2008) 914–915.
[61] R. Rakhi, M. Lekshmi, Electrochim. Acta 231 (2017) 539–548.
[62] X. Zhu, Y. Guo, H. Ren, C. Gao, Y. Zhou, Sens. Actuators B Chem. 248 (2017) 560–570.
[63] G. Zhang, T. Wang, X. Yu, H. Zhang, H. Duan, B. Lu, Nano Energy 2 (2013) 586–594.
[64] Y. Wang, H. Li, J. Zhang, X. Yan, Z. Chen, Phys. Chem. Chem. Phys. 18 (2016) 615–623.
[65] A. Venugopal, M.S. Scurrell, Appl. Catal. A Gen. 245 (2003) 137–147.
[66] M.A. Mellmer, C. Sener, J.M.R. Gallo, J.S. Luterbacher, D.M. Alonso, J.A. Dumesic, Angew. chem. int. ed 53 (2014) 11872–11875.
[67] K. Zhang, J.M. Suh, J.-W. Choi, H.W. Jang, M. Shokouhimehr, R.S. Varma, ACS Omega 4 (2019) 483–495.
[68] B. Elsler, A. Wiebe, D. Schollmeyer, K.M. Dyballa, R. Franke, S.R. Waldvogel, Chem. Eur. J. 21 (2015) 12321–12325.
[69] A.Ka. Lipeeka Rout, Rajendra S. Dhaka, G. Naaresh Reddya, Santanab Giri, P. Dash, Appl. Catal. A Gen. 538 (2017) 107–122.
[70] M. Shokouhimehr, K.-Y. Shin, J.S. Lee, M.J. Hackett, S.W. Jun, M.H. Oh, J. Jang, T. Hyeon, J. Mater. Chem. A Mater. Energy Sustain. 2 (2014) 7593–7599.
[71] C. Ma, Y. Wen, C. Rong, N. Zhang, J. Zheng, B.H. Chen, Catal. Sci.Tech. 7 (2017) 3200–3204.
[72] M. Nasrollahzadeh, B. Jaleh, A. Jabbari, RSC Adv. 4 (2014) 36713–36720.
[73] G. Ma, X. Yan, Y. Li, L. Xiao, Z. Huang, Y. Lu, J. Fan, J. Am. Chem. Soc. 132 (2010) 9596–9597.
[74] V. Idakiev, T. Tabakova, A. Naydenov, Z.-Y. Yuan, B.-L. Su, Appl. Catal. B 63 (2006) 178–186.
[75] Y.W. Changjian Ma, Chengli Rong, Nuowei Zhang, J.Za.B.H. Chen, Catal. Sci. Technol. 7 (2017) 3200–3204.
[76] L. Ding, C. Hao, Y. Xue, H. Ju, Biomacromolecules 8 (2007) 1341–1346.
[77] G. Ma, X. Yan, Y. Li, L. Xiao, Z. Huang, Y. Lu, J. Fan, J. Am. Chem. Soc. 132 (2010) 9596–9597.
[78] V. Idakiev, T. Tabakova, A. Naydenov, Z.-Y. Yuan, B.-L. Su, Appl. Catal. B 63 (2006) 178–186.
[79] D.-P. Yang, W. Guo, Z. Cai, Y. Chen, X. He, C. Huang, J. Zhuang, N. Jia, Sens. Actuators B Chem. 260 (2018) 642–649.
[80] K. Vinodgopal, B. Neppolian, I.V. Lightcap, F. Grieser, M. Ashokkumar, P.V. Kamat, J.Phys. Chem.lett. 1 (2010) 1987–1993.
[81] S. Zhang, W. Luo, X. Yang, T. Lv, Y. Huang, K. Dong, X. Li, Chem.select 2 (2017) 4557–4560.
[82] W. Guan, X. Chen, C. Li, J. Zhang, C.-W. Tsang, H. Hu, S. Li, C. Liang, Mol. Catal. 467 (2019) 61–69.
[83] X. Cui, W. Zuo, M. Tian, Z. Dong, J. Ma, Mol. Catal. 423 (2016) 386–392.
[84] W. Gu, X. Deng, X. Jia, J. Li, E. Wang, J. Mater.Chem. A 3 (2015) 8793–8799.
[85] L. Liu, A. Corma, Chem. Rev. 118 (2018) 4981–5079.
[86] J. Zhao, R. Jin, Nano Today 18 (2018) 86–102.
[87] M. Shokouhimehr, J.E. Lee, S.I. Han, T. Hyeon, Chem.Comm 49 (2013) 4779–4781.
[88] M. Shokouhimehr, J.E. Lee, S.I. Han, T. Hyeon, Chem.Comm. 49 (2013) 4779–4781.
[89] X. Li, C. Zeng, J. Jiang, L. Ai, J. Mater. Chem. 4 (2016) 7476–7482.
[90] M. Shokouhimehr, Y. Piao, J. Kim, Y. Jang, T. Hyeon, Angew. Chem.Int. Ed. 46 (2007) 7039–7043.
[91] H.-L. Shuai, K.-J. Huang, W.-J. Zhang, X. Cao, M.-P. Jia, Sens.Act. B 243 (2017) 403–411.